THE JOURNAL OF PHYSICAL CHEMISTRY A

Article

pubs.acs.org/JPCA

Electrochemical, Spectroscopic, and $^1O_2$ Sensitization Characteristics of 10,10-Dimethylbiladiene Complexes of Zinc and Copper

Allen J. Pistner,[§] Rachel C. Pupillo,[§] Glenn P. A. Yap,[§] Daniel A. Lutterman,[†] Ying-Zhong Ma,[†] and Joel Rosenthal*[,§]

[§]Department of Chemistry and Biochemistry, University of Delaware, Newark, Delaware 19716, United States

[†]Chemical Sciences Division, Oak Ridge National Laboratory, Oak Ridge, Tennessee 37831, United States

Supporting Information

ABSTRACT: The synthesis, electrochemistry, and photophysical characterization of a 10,10-dimethylbiladiene tetrapyrrole bearing ancillary pentafluorophenyl groups at the 5- and 15-*meso* positions (**DMBil1**) is presented. This nonmacrocyclic tetrapyrrole platform is robust and can serve as an excellent ligand scaffold for Zn^{2+} and Cu^{2+} centers. X-ray diffraction studies conducted for **DMBil1** along with the corresponding **Zn**[**DMBil1**] and **Cu**[**DMBil1**] complexes show that this ligand scaffold binds a single metal ion within the tetrapyrrole core. Additionally, electrochemical experiments revealed that all three of the aforementioned compounds display an interesting redox chemistry as the **DMBil1** framework can be both oxidized and reduced by two electrons. Spectroscopic and photophysical experiments carried out for **DMBil1**, **Zn**[**DMBil1**], and **Cu**[**DMBil1**] provide a basic picture of the electronic properties of these platforms. All three biladiene derivatives strongly absorb light in the visible region and are weakly emissive. The ability of these compounds to sensitize the formation of $^1O_2$ at wavelengths longer than 500 nm was probed. Both the free base and Zn^{2+} 10,10-dimethylbiladiene architectures show modest efficiencies for $^1O_2$ sensitization. The combination of structural, electrochemical, and photophysical data detailed herein provides a basis for the design of additional biladiene constructs for the activation of O_2 and other small molecules.

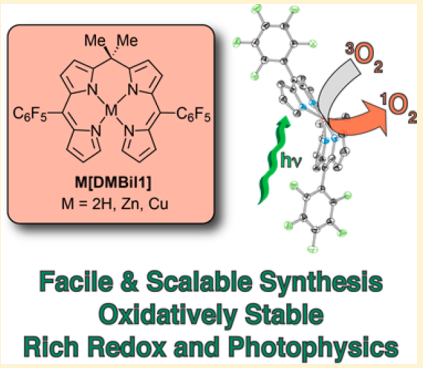

INTRODUCTION

Tetrapyrrole macrocycles such as porphyrins, corroles, and pthalocyanines are among the most well-studied class of organic chromophores and redox cofactors.[1] Linear tetrapyrroles such as biladienes and biliverdins have also been prepared and studied as organic chromophores with interesting absorption and photophysical properties.[2] Although linear polypyrroles do not typically absorb light as strongly as their conjugated macrocyclic homologues,[3] these chromophores serve an essential role in phytochrome photoreceptors, which work to regulate seed germination, flowering, and stem growth in plants.[4] In addition to serving several important roles in Nature, linear tetrapyrroles can also serve as ligands toward main group elements and transition metals[5] that include copper,[6,7] nickel,[8,9] and cobalt,[10,11] among others.[12] Although the coordination chemistry of several linear tetrapyrroles has received attention, the preparation and study of nonmacrocyclic tetrapyrrole complexes have not been pursued to nearly the same extent as porphyrinoid coordination chemistry.

The coordination chemistry of oligopyrroles has trailed that of porphyrinoids in part due to the preparation and study of linear tetrapyrrole derivatives having been hampered by their inherent instability. For example, a,c-biladiene derivatives in which two protons are connected to the sp^3-hybridized 10-position of the tetrapyrrole can rapidly decompose in the presence of light and air.[13] When the biladiene is unsubstituted at the 1- and 19-positions (the termini of the tetrapyrrole), decomposition often involves cyclization to generate the corresponding corrole macrocycle, which is aromatic and very stable (Scheme 1).[14−17] The inherent instability of most linear tetrapyrroles is reflected by the ease with which such systems can be oxidized as bilirubin and related compounds display several redox waves from ∼0.5−0.8 V versus SCE,[18] which is roughly 1 V lower than that observed for homologous porphyrinoid macrocycles.

Scheme 1. Cyclization of a,c-Biladienes to Generate Corroles

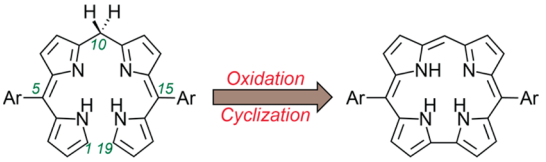

Special Issue: Current Topics in Photochemistry

Received: June 27, 2014
Revised: August 30, 2014
Published: September 4, 2014

   dx.doi.org/10.1021/jp506412r | J. Phys. Chem. A 2014, 118, 10639−10648

Given that deprotonation at the 10-position of the a,c-biladiene framework is required for cyclization and aromatization of the final corrole macrocycle,[19,20] addition of alkyl groups at the 10-position of the biladiene framework lends stability to this class of tetrapyrrole.[21] On the basis of this precedent, we rationalized that 10,10-dimethylbiladienes would represent a stable class of nonmacrocyclic tetrapyrroles that could serve as excellent ligands for transition-metal centers. Moreover, by adapting the synthetic methods developed for the preparation of phlorins[22−25] and other porphyrinoids[26−29] containing sp^3-hybridized *meso* positions, we sought to integrate pentafluorophenyl substituents onto the 5- and 15-positions of the biladiene framework. We now report that this strategy provides a convenient route to novel 10,10-dimethylbiladiene architectures that are easily metalated and offer a combination of chemical stability and synthetic availability. We have also characterized the structural, redox, and photophysical properties of these assemblies and show that they are modestly efficient sensitizers of $^1O_2$ using visible light.

EXPERIMENTAL SECTION

General Materials and Methods. Reactions were performed in oven-dried round-bottomed flasks unless otherwise noted. Reactions that required an inert atmosphere were conducted under a positive pressure of N_2 using flasks fitted with Suba-Seal rubber septa or in a nitrogen-filled glovebox. Air- and moisture-sensitive reagents were transferred using standard syringe or cannula techniques. Reagents and solvents were purchased from Sigma-Aldrich, Acros, Fisher, Strem, or Cambridge Isotopes Laboratories. Solvents for synthesis were of reagent grade or better and were dried by passage through activated alumina and then stored over 4 Å molecular sieves prior to use.[30] 5,5-Dimethyldipyrromethane and 5,5-dimethyl-1,9-bis(pentafluorobenzoyly)-dipyrromethane were prepared using previously described methods.[22−25] All other reagents were used as received.

Compound Characterization. ^1H NMR and ^{13}C NMR spectra were recorded at 25 °C on a Bruker 400 MHz spectrometer. Proton spectra are referenced to the residual proton resonance of the deuterated solvent ($CDCl_3$ = δ 7.26), and carbon spectra are referenced to the carbon resonances of the solvent ($CDCl_3$ = δ 77.16).[31] All chemical shifts are reported using the standard δ notation in parts-per-million; positive chemical shifts are to higher frequency from the given reference. LR-GCMS data were obtained using an Agilent gas chromatograph consisting of a 6850 Series GC system equipped with a 5973 Network mass-selective detector. LR-ESI MS data were obtained using either a LCQ Advantage from Thermofinnigan or a Shimadzu LCMS-2020. High-resolution mass spectrometry analyses were performed by the Mass Spectrometry Laboratory in the Department of Chemistry and Biochemistry at the University of Delaware.

10,10-Dimethyl-5,15-dipentfluorophenylbiladiene (DMBil1). To a solution of 5,5-dimethyl-1,9-bis-(pentafluorobenzoyly)-dipyrromethane (**1**) (281 mg, 0.50 mmol) dissolved in 40 mL of THF and MeOH (3:1) was added 946 mg of $NaBH_4$ (25.0 mmol). The $NaBH_4$ was added as a solid in a single batch at room temperature. The resulting mixture was stirred at room temperature for 2 h, following which the reaction was quenched with H_2O and extracted with dichloromethane. The organic layer was washed sequentially with H_2O and brine and dried over Na_2SO_4. The solvent was then removed via rotary evaporation, and the resulting residue was dissolved in 200 mL of dichloromethane and combined with $InCl_3$ (15 mg, 68 μmol) and pyrrole (100 μL, 1.44 mmol). The reaction was stirred at room temperature under air for 30 min, after which time 180 mg of DDQ (0.8 mmol) was added to the stirred solution. After stirring the reaction for an additional 5 min, 14 mL of triethylamine (100 mmol) was added, and the mixture was stirred for an additional 2 h. Following removal of the solvent under reduced pressure, the crude product was purified by chromatography on silica using a mixture of hexanes and CH_2Cl_2 (2:1) as the eluent to give 160 mg of the title compound in 53% yield. ^1H NMR (400 MHz, $CDCl_3$, 25 °C) δ/ppm: 12.43 (s, 2H), 7.18 (s, 2H), 6.63 (d, J = 4.6 Hz, 2H), 6.57 (d, J = 4.6 Hz, 2H), 6.29−6.24 (m, 2H), 6.22 (d, J = 3.7 Hz, 2H), 1.81 (s, 6H). ^{13}C NMR (101 MHz, $CDCl_3$, 25 °C) δ/ppm: 177.47, 148.05, 144.98 (d, J = 248 Hz), 141.58 (d, J = 254 Hz), 137.55 (d, J = 252 Hz), 133.02, 132.27, 130.45, 124.61, 122.00, 120.24, 112.62, 111.68, 42.16, 26.00. HR-LIFDI-MS $[M]^+$ m/z: calcd for $C_{33}H_{18}N_4F_{10}$, 660.1372; found, 660.1372. Anal. Calcd for $C_{33}H_{18}F_{10}N_4$: C, 60.01; H, 2.75; N, 8.48. Found: C, 59.60; H, 3.04; N, 8.17.

Zn[DMBil1]. To a solution of **DMBil1** (100 mg, 0.15 mmol) dissolved in 30 mL of DMF was added 665 mg of $Zn(OAc)_2$ (3 mmol). This solution was heated at 60 °C for 4 h. Following removal of the solvent under reduced pressure, the resulting residue was dissolved in CH_2Cl_2 and filtered through Celite. The filtrate was washed with brine and dried over Na_2SO_4. Following removal of the CH_2Cl_2 by rotary evaporation, the crude product was redissolved in MeOH and concentrated under reduced pressure to deliver 76 mg of the title compound in 70% yield. ^1H NMR (400 MHz, $CDCl_3$, 25 °C) δ/ppm: 7.12 (s, 2H), 6.58 (d, J = 4.1 Hz, 2H), 6.54 (d, J = 3.9 Hz, 2H), 6.50 (d, J = 4.2 Hz, 2H), 6.38 (d, J = 3.7 Hz, 2H), 1.74 (s, 6H). ^{13}C NMR (101 MHz, $CDCl_3$) δ: 170.55, 150.72, 144.85 (d, J = 248.7 Hz), 141.22 (d, J = 248.7 Hz), 141.07, 139.75, 137.20 (d, J = 253.1 Hz), 131.44, 129.23, 128.15, 116.90, 116.54, 39.43, 30.21. HR-EI-MS $[M]^+$ m/z: calcd for $C_{33}H_{16}N_4F_{10}Zn$, 722.05064; found, 722.04983. Anal. Calcd for $C_{33}H_{16}F_{10}N_4Zn$ + 1/2 CH_3OH + DMF: C, 54.42; H, 2.89; N, 8.05. Found: C, 54.23; H, 2.57; N, 7.94.

Cu[DMBil1]. To a solution of **DMBil1** (100 mg, 0.15 mmol) dissolved in 40 mL of CH_3CN was added 45 mg of $Cu(OAc)_2$ (0.225 mmol). This solution was heated to 60 °C for 4 h. Following removal of the solvent under reduced pressure, the crude material was purified by chromatography on silica using hexane and CH_2Cl_2 (2:1) as the eluent to give 100 mg of the title compound in 92% yield. HR-ESI-MS $[M + H]^+$ m/z: calcd for $C_{33}H_{17}N_4F_{10}Cu$, 722.0590; found, 722.0595. Anal. Calcd for $C_{33}H_{16}F_{10}N_4Cu$: C, 54.89; H, 2.23; N, 7.76. Found: C, 54.90; H, 2.01; N, 7.48.

Steady-State Spectroscopy. UV/visible absorbance spectra were acquired on a StellarNet CCD array UV−vis spectrometer using screw cap quartz cuvettes (7q) of 1 cm path length from Starna. All absorbance spectra were recorded at room temperature. All samples for spectroscopic analysis were prepared in dry CH_2Cl_2 within a N_2-filled glovebox.

Steady-state fluorescence spectra were recorded on an automated Photon Technology International (PTI) QuantaMaster 40 fluorometer equipped with a 75 W xenon arc lamp, an LPS-220B lamp power supply, and a Hamamatsu R2658 photomultiplier tube. Samples for fluorescence analysis were prepared in an analogous method to that described above for the preparation of samples for UV−vis spectroscopy. Samples of **DMBil1**, **Zn(DMBil1)**, and **Cu(DMBil1)** were excited at λ_{ex}

= 450, 475, and 465 nm, respectively, and emission was monitored with a step size of 0.5 nm and integration time of 0.25 s. Reported spectra are the average of at least five individual acquisitions.

Emission quantum yields were calculated using $[Ru(bpy)_3]Cl_2$ in acetonitrile (Φ_{ref} = 0.062)[32,33] as the reference actinometer using the expression below[33]

$$\Phi_{em} = \Phi_{ref}\left(\frac{A_{ref}}{A_{em}}\right)\left(\frac{I_{em}}{I_{ref}}\right)\left(\frac{\eta_{em}}{\eta_{ref}}\right)^2$$

where Φ_{em} and Φ_{ref} are the emission quantum yield of the sample and the reference, respectively, A_{ref} and A_{em} are the measured absorbances of the reference and sample at the excitation wavelength, respectively, I_{ref} and I_{em} are the integrated emission intensities of the reference and sample, respectively, and η_{ref} and η_{em} are the refractive indices of the solvents of the reference and sample, respectively.

Time-Resolved Spectroscopy. Picosecond time-correlated single-photon counting (TCSPC) measurements were performed using a commercial femtosecond Ti:sapphire oscillator (Coherent Mira 900F) as the light source, which generates frequency-tunable pulses with a typical full width at half-maximum (fwhm) of 150 fs and a 76 MHz repetition rate. The output at a selected central wavelength was frequency-doubled using a 1.5 mm thick BBO crystal to obtain the excitation pulses centered at ~455 nm. Fluorescence emission was selected using a 10 nm (fwhm) band-pass filter centered at 520 nm for **DMBil1** and at 540 nm for **Zn**[**DMBil1**], which were chosen according to the peak wavelengths of their fluorescence emission spectra. The detection system has been described in detail previously,[34] which involves an actively quenched single-photon avalanche photodiode (PDM 50CT module, Micro Photon Devices) and a TCSPC module (PicoHarp 300, PicoQuant). The instrument response function (IRF) showed a fwhm of 70 ps as recorded using a dilute water suspension of coffee creamer directly at these chosen detection wavelengths to avoid pronounced spectral dependence of the detector in the spectral region of our interest. A 4.0 ps channel time was chosen, and at least 7000 counts were collected in the peak channel for the samples in order to obtain an acceptable signal-to-noise ratio. The polarization of the excitation beam was set to the magic angle (54.7°) with respect to an emission linear polarizer, which eliminates any depolarization contribution. Quantitative analysis of the time-resolved fluorescence data was performed by employing a least-squares deconvolution fitting algorithm with explicit consideration of the finite IRF (FluoFit, PicoQuant), and a reduced chi-squares (χ^2) value was used to judge the quality of each fit.

Singlet Oxygen Sensitization. Quantification of singlet oxygen generation was carried out using the fluorescent probe 1,3-diphenylisobenzofuran as a trapping agent for $^1O_2$.[35] Fluorescence measurements were recorded for CH_3OH solutions that were 10 μM in sensitizer and 10 μM in 1,3-diphenylisobenzofuran. The solutions (2.0 mL total volume) were contained in screw cap quartz cuvettes (7q) of 1 cm path length and were irradiated with light passed through either a 500 or 550 nm band-pass filter. The rate of $^1O_2$ production was determined by monitoring consumption of the 1,3-diphenylisobenzofuran. This was accomplished by determining the decrease in integrated emission intensity from unreacted furan every 5 min for a total of 30 min. $^1O_2$ sensitization quantum yields were determined using $[Ru(bpy)_3]Cl_2$ (Φ_{ref} = 0.81 in CH_3OH) as a reference sensitizer and the expression below, where $\Phi_{^1O_2}$ and Φ_{ref} are the singlet oxygen sensitization quantum yields for the sample and reference, respectively, m_{sample} and m_{ref} are the slopes of the decrease in furan fluorescence for the sample and the reference, respectively, and ε_{sample} and ε_{ref} are the molar absorptivities at the irradiation wavelength (500 nm) for the sample and reference, respectively.

$$\Phi_{^1O_2} = \Phi_{ref}\left(\frac{m_{sample}}{m_{ref}}\right)\left(\frac{\varepsilon_{ref}}{\varepsilon_{sample}}\right)$$

Electrochemistry. Cyclic voltammetry (CV) experiments were performed in a N_2-filled glovebox using a CHI-620D potentiostat and a standard three-electrode assembly. CV scans were recorded for quiescent solutions using a platinum working disk electrode (2.0 mm diameter), a platinum wire auxiliary electrode, and a silver wire quasi-reference electrode. CV experiments were performed in MeCN containing 0.1 M tetrabutylammonium hexafluorophosphate ($TBAPF_6$) as the supporting electrolyte. Concentrations of analyte were 1 mM, and a scan rate of 50 mV/s and sensitivity of 10 mA/V were maintained during data acquisition. All reported potentials are referenced relative to Ag/AgCl using a decamethylferrocenium−decamethylferrocene internal standard of 1 mV versus Ag/AgCl.[36]

X-ray Structural Solution and Refinement. X-ray structural analysis for **DMBil1**, **Zn**[**DMBil1**], and **Cu**[**DMBil1**]: Crystals were mounted using viscous oil onto a plastic mesh and cooled to the data collection temperature. Data were collected on a Bruker-AXS APEX 2 DUO CCD diffractometer with Cu Kα radiation (λ = 1.54178 Å) collimated and monochromated using Goebel mirrors or with Mo Kα radiation (λ = 0.71073 Å) monochromated with a graphite crystal. Unit cell parameters were obtained from 36 data frames, 0.5° ω, from three different sections of the Ewald sphere. No higher symmetry than triclinic was observed for **DMBil1** and **Zn**[**DMBil1**]. Solution in *P*-1 yielded chemically reasonable and computationally stable results of refinement. The unit cell parameters and systematic absences in the diffraction data for **Cu**[**DMBil1**] are consistent with $Pna2_1$ and *Pnam* [*Pnma*]. However, the observed occupancy and the absence of either a molecular mirror or a molecular inversion center are consistent exclusively with the noncentrosymmetric space group, $Pna2_1$. The absolute structure parameter in **Cu**[**DMBil1**] refined to nil, indicating the true hand of the data, has been determined. An inspection of the packing diagram suggests no overlooked symmetry. The data sets were treated with numerical absorption corrections based on indexed crystal faces and dimensions (Apex2 software suite, Madison, WI, 2005). The structures were solved using direct methods and refined with full-matrix, least-squares procedures on F^2.[37] A P−M pseudohelical isomer pair, with a 3.4 Å π−π offset parallel intermolecular distance, and severely disordered solvent molecules (two ethanol molecules and two chloroform molecules, one of which was located near the origin at half-occupancy) were located in the asymmetric unit of **Zn**[**DMBil1**]. Cocrystallized, noncoordinated, solvent molecules in **Zn**[**DMBil1**] were treated as diffused diffraction contributions using Squeeze.[38] All non-hydrogen atoms were refined with anisotropic displacement parameters. The amine hydrogen atoms in **Zn**[**DMBil1**] were assigned to be consistent with surrounding non-hydrogen atom geometry and allowed to

dx.doi.org/10.1021/jp506412r | J. Phys. Chem. A 2014, 118, 10639−10648

Scheme 2. Synthesis and Metallation of 10,10-Dimethylbiladiene

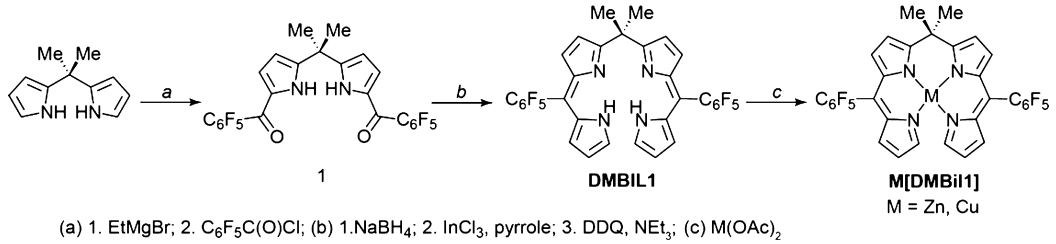

(a) 1. EtMgBr; 2. $C_6F_5C(O)Cl$; (b) 1.$NaBH_4$; 2. $InCl_3$, pyrrole; 3. DDQ, NEt_3; (c) $M(OAc)_2$

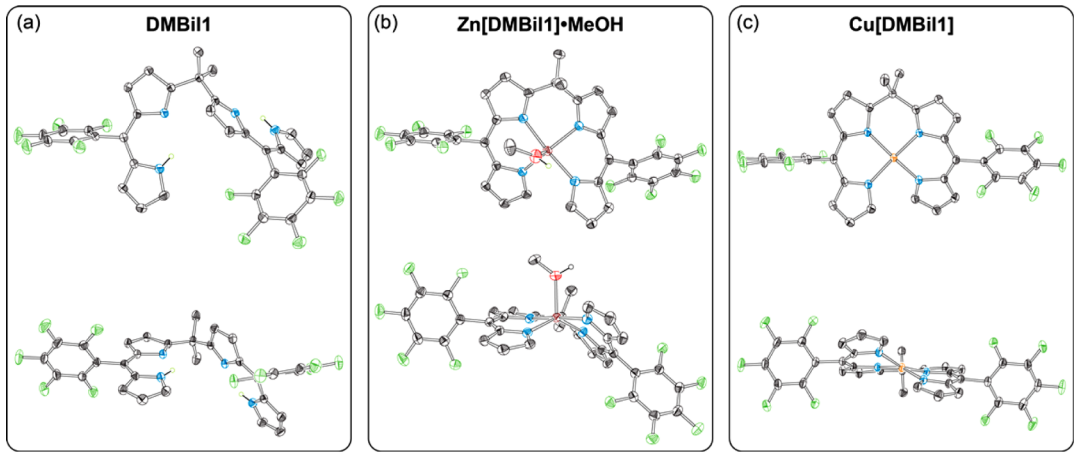

Figure 1. Comparative views of crystal structures of (a) **DMBIL1**, (b) **Zn[DMBil1]·MeOH**, and (c) **Cu[DMBil1]**. Thermal ellipsoid plots are shown from above (top) and in profile (bottom) for each structure. Ellipsoids are drawn at the 50% probability level. Hydrogen atoms (except those on coordinated solvent molecules) are omitted for clarity.

Table 1. Crystallographic data for DMBil1, Zn[DMBil1] and Cu[DMBil1]

	DMBil1	Zn[DMBil1]·CH_3OH	Cu[DMBil1]
formula	$C_{33}H_{18}F_{10}N_4$	$C_{34}H_{20}F_{10}N_4OZn$	$C_{33}H_{16}F_{10}N_4Cu$
F_w	660.5	877.48	722.04
crystal system	triclinic	triclinic	orthorhombic
space group	*P*-1	*P*-1	*Pna*2(1)
a (Å)	9.762(2)	9.4815(3)	10.4143(3)
b (Å)	9.830(2)	14.8240(5)	19.3742(5)
c (Å)	15.163(4)	26.6756(10)	14.0031(4)
α (deg)	100.996(4)	104.113(2)	90
β (deg)	93.420(4)	98.585(2)	90
γ (deg)	96.674(4)	91.238(2)	90
V (Å^3)	1414.7(6)	3588.9(2)	2825.39(14)
Z	2	4	4
temp (K)	200(2)	200(2)	200(2)
D_{calcd} (g/cm^{-3})	1.551	1.624	1.697
2θ range (deg)	4.22−54.92	6.92−147.66	7.78−136.46
μ (Mo Kα) (mm^{-1})	0.139	3.326	1.999
relections	18532	116052	15559
unique	6426	13894	4610
R(int)	0.0235	0.0683	0.0182
R_1	0.0396	0.0424	0.237
wR_2	0.0924	0.1080	0.0659

refine in position but with the anisotropic parameter restrained to 1.2 U_{eq} of the attached nitrogen atom. All other hydrogen atoms were treated as idealized contributions. Atomic scattering factors are contained in the SHELXTL 6.12 program library. The CIF has been deposited under CCDC 996931-996933.

Computations. All density functional calculations were performed using the Gaussian 09 (G09) program package,[39] with the Becke three-parameter hybrid exchange and Lee−Yang−Parr correlation functional (B3LYP).[40−42] The 6-31G* basis set was used for C, N, and F atoms. The LANL2DZ[43] pseudopotential was used for Zn. All calculations used the SMD universal continuum model[44] with CH_2Cl_2 as the solvent (ε = 8.93). All geometry optimizations were performed in C_1 symmetry with subsequent vibrational frequency analysis to

dx.doi.org/10.1021/jp506412r | J. Phys. Chem. A 2014, 118, 10639−10648

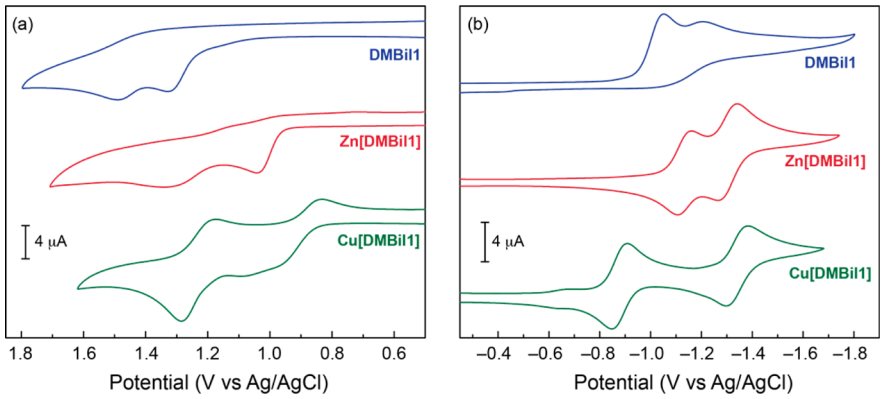

Figure 2. (a) Oxidative and (b) reductive cyclic voltammograms (CVs) recorded at a scan rate of 50 mV/s for **DMBil1**, **Zn**[**DMBil1**], and **Cu**[**DMBil1**] in MeCN containing $TBAPF_6$ and an internal decamethylferrocene standard.

confirm that each stationary point was a minimum on the potential energy surface. The vertical singlet transition energies of the complexes were computed at the time-dependent density functional theory (TD-DFT) level in CH_2Cl_2 within G09 by using the optimized ground-state structure.

RESULTS AND DISCUSSION

Biladiene Synthesis. Synthesis of a 10,10-dimethylbiladiene ligand with aryl groups at the 5- and 15-positions is straightforward, as illustrated in Scheme 2. This synthesis starts with condensation of 5,5-dimethyldipyrromethane with pentafluorophenylbenzoyl chloride to yield the corresponding diacylated compound (**1**) in 30% yield.[22] The subsequent reaction with pyrrole using TFA as an acid catalyst neatly yields the free base dimethylbiladiene with ancillary C_6F_5 substituents (**DMBil1**).

Metalation of the biladiene ligand is readily accomplished by reaction with divalent metal acetates. Treatment of **DMBil1** with $Zn(OAc)_2{\cdot}2H_2O$ in DMF at 60 °C for 4 h cleanly affords the corresponding zinc(II) complex (**Zn**[**DMBil1**]) in 70% yield. The **Zn**[**DMBil1**] complex was characterized using a combination of ^1H and ^{13}C NMR, high-resolution mass spectrometry, and elemental analyses. The homologous biladiene complex of copper(II) (**Cu**[**DMBil1**]) is similarly obtained in fine yield upon reaction of **DMBil1** with $Cu(OAc)_2{\cdot}2H_2O$ in MeCN. Characterization of **Cu**[**DMBil1**] provided satisfactory mass spectrometry and elemental analyses.

Structural Characterization of DMBil1. The solid-state structures of **DMBil1**, **Zn**[**DMBil1**] and **Cu**[**DMBil1**] are shown in Figure 1, and crystallographic parameters for each structure are provided in Table 1. Each of the atoms that make up the core of the free base biladiene ligand and metal complexes is numbered in the standard fashion (note: fully labeled and numbered thermal ellipsoid plots of **DMBil1**, **Zn**[**DMBil1**], and **Cu**[**DMBil1**] are provided in the Supporting Information), and structural metrics for these systems are tabulated in Tables S1−S6. Structural highlights of the crystal structures obtained for the systems studied are summarized below.

The 10,10-dimethylbiladiene tetrapyrrole ligand is conformationally flexible, and the dipyrromethane units are significantly distorted from coplanarity in the solid-state structure of **DMBil1**. The dihedral angle between the two dipyrromethane units bridged by the saturated dimethyl-substituted sp^3 center is 66.08°. This bent structure is consistent with calculated global energy minima for related 1,19-unsubstituted a,c-biladienes, for which the planar corrole-like conformation has been predicted to be roughly 20 kcal/mol higher in energy.[45] The pentafluorophenyl substituents are also canted with respect to the planes of the individual dipyrromethane moieties with average dihedral angles of 67.57°. Finally, the alternating short and long bond lengths of the pyrroles adjoined through the central sp^3 hybridized center (C(10)) are consistent with the tautomeric structure shown in Figure 1, in which the terminal pyrrole positions bear protonated nitrogens. The C(1)−N(1) versus C(4)−N(1) and C(30)−N(4) versus C(33)−N(4) bond distances differ slightly by 0.029 and 0.017 Å, respectively, consistent with the assigned protonation.

Metalation of **DMBil1** leads to coordination by all four pyrrole moieties of the biladiene ligand bind to a single central metal. **Zn**[**DMBil1**]**·CH$_3$OH** (Figure1b, Table 1) is formed upon crystallization of the zinc(II) complex from a concentrated solution of $CHCl_3$ and CH_3OH (1:1). Under these crystallization conditions, 1 equiv of methanol is bound to the metal with trigonal bipyramidal coordination geometry. The equatorial plane of **Zn**[**DMBil1**]**·MeOH** is comprised of pyrrole nitrogen atoms, N(2) and N(4), and the methanol ligand. The overall structure of **Zn**[**DMBil1**]**·MeOH** is reminiscent of a previously reported zinc octaethylformylbiliverdinate complex bearing an apical aquo ligand;[46] however, because the bilverdinate ligand is conjugated across all four pyrrole units, this tetrapyrrole complex adopts a square-pyramidal geometry instead. The structure of **Zn**[**DMBil1**]**·MeOH** is also distinct from that reported for a zinc complex of decamethyl-a,c-biladiene, which does not have a bound solvato ligand in the apical position.[47]

Binding of zinc(II) to the **DMBil1** ligand leads to desymmetrization of the 10,10-dimethyl substituents. The six-membered ring comprised of Zn(1), N(2), C(15), C(10), C(19), and N(3) adopts a distorted boat-type conformation, resulting in C(18) being projected into an axial position and C(17) into an equatorial position. Moreover, the C(10)−C(18) bond is canted by only 25.22° with respect to the Zn(1)−O(1) axis that defines the zinc−methanol bond. The dihedral angle between the two pyrroles bridged by the saturated dimethyl-substituted sp^3 center (C(10)) is significantly compressed (16.55°) in comparison to that for the free base ligand (vide supra). Nonetheless, the biladiene ligand is still highly distorted from a planar corrole-like conformation as the two terminal pyrrole units that make up the ligand are canted by 48.40° with respect to one another due to steric

dx.doi.org/10.1021/jp506412r | J. Phys. Chem. A 2014, 118, 10639−10648

Table 2. Photophysical and Electrochemical Data for DMBil1, Zn[DMBil1] and Cu[DMBil1]

compound	$E_{ox}(1,2)$/V	$E_{red}(1,2)$/V	λ_{abs}/nm ($\varepsilon \times 10^3$ $M^{-1}\cdot cm^{-1}$)	λ_{em}/nm (Φ_{em})	$\Phi_{^1O_2}$
DMBil1	1.33, 1.49	−1.05, −1.21	291(1.1), 423(41.4), 450(43.0)	543(1.7×10^{-3})	1.5×10^{-2}
Zn[DMBil1]	1.04, 1.33	−1.13, −1.31	306(6.9), 368(6.6), 467(50.8), 513(8.2), 548(10.2)	573(7.0×10^{-4})	2.6×10^{-2}
Cu[DMBil1]	0.92, 1.24	−0.88, −1.34	308(11.2), 364(13.0), 474(59.4), 558(9.1)		$<0.2 \times 10^{-2}$

clashing between H(33) and C(1). As a result, C(1) and C(33) are separated by over 3.3 Å.

The copper(II) center of **Cu[DMBil1]** is four-coordinate; however, unlike in most typical copper(II) porphyrinoids, the coordination environment is significantly distorted from square-planar. Similar to the case for the **Zn[DMBil1]** derivative, steric repulsion between H(1A) and C(19) as well as H(19A) and C(1) on the terminal pyrroles causes the entire biladiene scaffold to twist. Atoms C(1) and C(19) are therefore separated by ∼3.04 Å, although this distance is closer than the two corresponding carbon atoms for the zinc(II) derivative by more than 0.25 Å. Similarly, the two terminal pyrrole units that make up the tetrapyrrole platform are canted by 50.59° with respect to one another. The bond distances between the copper(II) center and pyrrole nitrogens range from 1.969 to 1.980 Å, with an average distance of ∼1.972 Å. The ancillary pentafluorophenyl substituents are nearly orthogonal with respect to the planes of the individual dipyrromethane moieties that make up the biladiene scaffold of **Cu[DMBil1]**, with average dihedral angles of 82.57°.

Electrochemistry. Polypyrrole scaffolds display rich redox properties and can often be oxidized and/or reduced by multiple electron equivalents. CV carried out for 1.0 mM solutions of **DMBil1** in MeCN containing 0.1 M $TBAPF_6$ shows that the biladiene can be both oxidized and reduced by two electrons. The CV trace recorded for **DMBil1** (blue trace) is shown in Figure 2 and displays two irreversible one-electron oxidation ($E_{ox}(1) \approx 1.33$ V, $E_{ox}(2) \approx 1.49$ V) and two irreversible one-electron reduction waves ($E_{red}(1) \approx -1.05$ V, $E_{red}(2) \approx -1.21$ V). These redox properties are significantly perturbed upon metalation of the biladiene scaffold with either zinc or copper. Figure 2 juxtaposes the CV traces recorded for **Zn[DMBil1]** (red trace) and **Cu[DMBil1]** (green trace) with the free base biladiene (**DMBil1**). Both the zinc and copper biladiene scaffolds also display four one-electron redox waves that include two oxidation events. As summarized in Table 2, **Zn[DMBil1]** displays two irreversible one-electron oxidations at $E_{ox}(1) \approx 1.04$ V and $E_{ox}(2) \approx 1.33$ V. **Cu[DMBil1]** also displays two oxidation waves ($E_{ox}(1) \approx 0.92$ V and E_{ox} (2) ≈ 1.24 V), which are more reversible than those observed for the zinc or free base biladiene derivatives. It is unclear as to why the oxidation of **Cu[DMBil1]** is more reversible on the CV time scale when compared to the oxidation of the free base and **Zn[DMBil1]** derivatives.

In contrast to the free base biladiene ligand, both **Zn[DMBil1]** and **Cu[DMBil1]** display reversible reductive redox events. **Zn[DMBil1]** displays two reversible one-electron reduction events at $E_{red}(1) \approx -1.13$ V and $E_{red}(2) \approx -1.31$ V, and **Cu[DMBil1]** displays two reversible one-electron reduction events at $E_{red}(1) \approx -0.88$ V and $E_{red}(2) \approx -1.34$ V. Given that the two reductive redox couples observed for each of the above **DMBil1** derivatives occur at similar potentials, it is likely that both reductive waves observed for the **Zn[DMBil1]** and **Cu[DMBil1]** complexes correspond to reduction of the tetrapyrrole ligand. We note that while the $E_{red}(2)$ values obtained for both the Zn^{2+} and Cu^{2+} biladiene derivatives are centered at around −1.3 V, the first reduction of these two derivatives occurs at vastly different potentials. As shown in Figure 2b, **Cu[DMBil1]** displays an $E_{red}(1)$ value that is ∼0.25 V more positive than that recorded for **Zn[DMBil1]**. This difference may be due to adsorption of the **Cu[DMBil1]** at the electrode surface upon reduction, as judged by the broad polarization features that are observed in the CV for this compound from −0.55 to −0.75 V (Figure 2b).

Spectroscopy. Electronic spectra of **DMBil1** and its zinc(II) and copper(II) complexes are consistent with other tetrapyrrole frameworks containing a point of saturation. Figure 3 compares the electronic absorption spectra of **DMBil1**, **Zn[DMBil1]**, and **Cu[DMBil1]** in CH_2Cl_2. The spectral profile of **DMBil1** is reminiscent of that of homologous tetrapyrroles with a 5,5-diproteo substitution pattern. For instance, similar to **DMBil1**, the free base form of 1,19-dideoxybiladienes-ac demonstrates a strong absorption at roughly 520 nm with weaker bands at wavelengths between

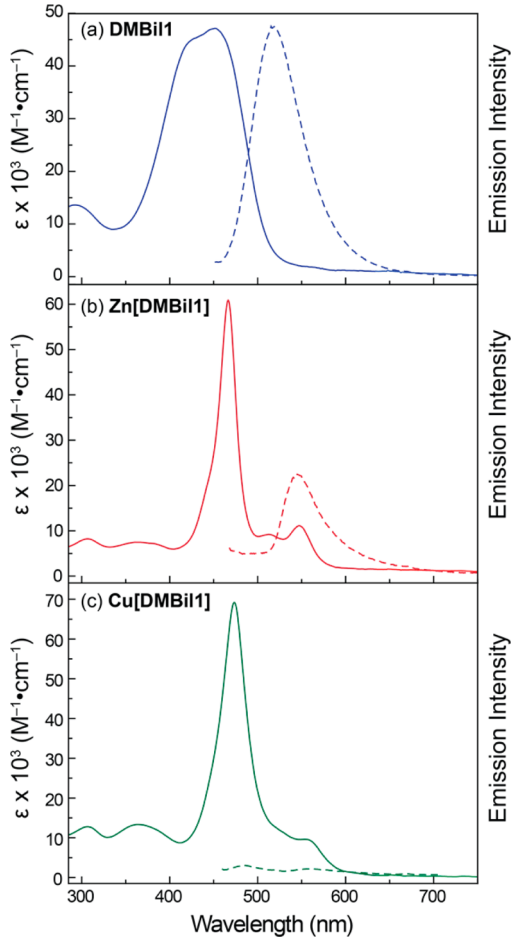

Figure 3. Electronic absorption (solid curves) and emission (dashed curves) spectra recorded at 298 K in CH_2Cl_2 of (a) **DMBil1**, (b) **Zn[DMBil1]**, and (c) **Cu[DMBil1]**.

dx.doi.org/10.1021/jp506412r | J. Phys. Chem. A 2014, 118, 10639−10648

300 and 400 nm.[19] By comparison, **DMBil1** displays two closely separated, strongly absorbing bands at 423 ($\varepsilon \approx 41\,480$) and 450 nm ($\varepsilon \approx 43\,060$). TD-DFT calculations performed for this tetrapyrrole derivative revealed that these intense absorption bands are correlated to transitions between the four molecular frontier orbitals. As shown in Figure 4, both of these $\pi-\pi^*$ transitions involve the near-degenerate HOMO and HOMO−1 levels, as well as the LUMO and LUMO+1.

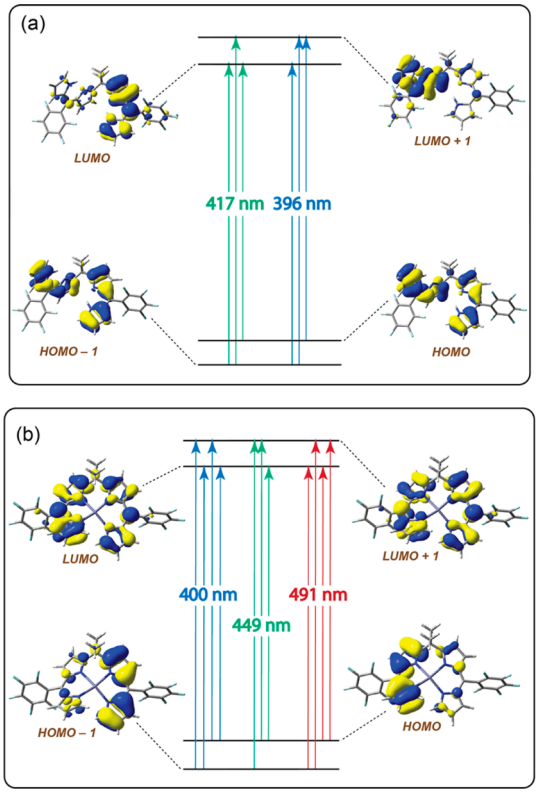

Figure 4. Representation of the molecular orbitals involved in the major electronic absorption transitions for (a) **DMBil1** and (b) **Zn**[**DMBil1**] in CH_2Cl_2.

Metalation of the **DMBil1** scaffold with Zn^{2+} is manifest in significant changes to the structure and corresponding electronic absorption spectrum of this chromophore. As opposed to the free base **DMBil1** ligand, which displays two intense bands of similar intensity between ~420 and 450 nm, CH_2Cl_2 solutions of **Zn**[**DMBil1**] display a single intense transition at 467 nm (ε = 50 790). TD-DFT calculations indicate that this absorption is largely attributable to electronic transitions between the four frontier orbitals between the HOMO−1 and LUMO+1. The electron density of the molecular orbitals is confined to the biladiene π-system. In contrast to the free ligand, **Zn**[**DMBil1**] also displays two low-energy absorptions at 513 (ε = 8180) and 548 nm (ε = 10 170). These absorption bands are weaker than the primary $\pi-\pi^*$ transition at 467 nm but serve to extend the ability of the chromophore to absorb light at longer wavelengths. TD-DFT calculations revealed that the two low-energy transitions observed for **Zn**[**DMBil1**] can be primarily attributed to electron promotion from the near-degenerate HOMO and HOMO−1 levels to the closely spaced LUMO and LUMO+1. The UV−vis absorption profile of **Cu**[**DMBil1**] is qualitatively similar to that of the corresponding Zn^{2+} derivative. The photophysical properties of the **DMBil1** derivatives detailed above are summarized in Table 2.

Not unlike other tetrapyrrole derivatives, **DMBil1** produces strong fluorescence upon photoexcitation. Excitation into the absorption bands of **DMBil1** induces a broad emission profile between approximately 500 and 700 nm that is centered at 543 nm (τ_{obs} = 15.3 ps). The quantum yield for emission upon excitation of **DMBil1** in deaerated CH_2Cl_2 at λ_{ex} = 450 nm is $\Phi_{DMBIL1} = 1.7 \times 10^{-3}$. **Zn**[**DMBil1**] is also luminescent (τ_{obs} = 22.3 ps); however, the emission from this zinc complex is shifted to lower energies compared to the free base biladiene ligand. The fluorescence lifetimes of **DMBil1** and **Zn**[**DMBil1**] are significantly shorter than analogous porphyrin derivatives, which typically range from approximately 2 to 15 ns at room temperature in typical organic solvents.[48] The emission lifetimes recorded for **DMBil1** and **Zn**[**DMBil1**] are similar in value to those observed for phlorin tetrapyrrole architectures that contain a single sp^3 hybridized *meso* position.[22−25]

Similar to the trend observed for zinc versus free base porphyrins, the quantum yield for emission from **Zn**[**DMBil1**] is reduced by more than 50% to $\Phi_{Zn[DMBIL1]} = 7.0 \times 10^{-4}$ as compared to the value observed for **DMBil1**. The emission observed for **DMBil1** and **Zn**[**DMBil1**] is presumed to originate from the excited singlet state of these compounds because the emission quantum yields are not attenuated by introduction of oxygen to the luminescent samples. Incorporation of Cu^{2+} into the biladiene core abolishes the luminescence observed for this platform. This observation is typical of tetrapyrrole complexes with open d shells, as the placement of d−d states energetically below the $\pi-\pi$ states of the conjugated ligand circumvents luminescence for **Cu**[**DMBil1**].

Sensitized Production of $^1O_2$. Porphyrinoids have found application for the sensitization of $^1O_2$, which is the reactive species produced by many light-absorbing agents that are employed for photodynamic therapy (PDT).[49−54] Furthermore, many tetrapyrrole derivatives that contain points of saturation along the ligand backbone are particularly good sensitizers of $^1O_2$ upon excitation with light toward the low-energy end of the visible region of the electromagnetic spectrum.[55−59] As such, we rationalized that biladiene complexes may also be able to serve in such a role.

The quantum yields for sensitization of $^1O_2$ by **DMBil1**, **Zn**[**DMBil1**], and **Cu**[**DMBil1**] were measured using $[Ru(bpy)_3]^{2+}$ as a standard ($\Phi_{^1O_2}$ = 0.81 in CH_3OH)[60] and 1,3-diphenylisobenzofuran as a trapping agent for the detection of $^1O_2$.[35,61] The quantum yield of $^1O_2$ sensitization by **DMBil1** in CH_3OH was measured to be $\Phi_{^1O_2} = 1.5 \times 10^{-2}$ upon irradiation at λ_{irr} = 500 nm. Although this quantum yield is only modest, when compared to free base porphyrin architectures, which can sensitize the production of $^1O_2$ with quantum efficiencies that approach $\Phi_{^1O_2}$ = 0.8 in polar protic solvents,[58,62] our results clearly demonstrate that the 10,10-dimethylbiladiene tetrapyrrole can be used to generate $^1O_2$. Because the absorbance profile of **Zn**[**DMBil1**] displays spectral features from 500 to 575 nm, this complex provides a means to sensitize $^1O_2$ production using longer-wavelength light than that required for the free base **DMBil1** ligand. The value of $\Phi_{^1O_2}$ for **Zn**[**DMBil1**] was measured to be 2.6×10^{-2} in CH_3OH (λ_{irr} = 550 nm). The enhanced photosensitization observed for the zinc derivative likely stems in part from the presence of the Zn^{2+} center, which enhances the kinetics and efficiency with

dx.doi.org/10.1021/jp506412r | J. Phys. Chem. A 2014, 118, 10639−10648

which the **DMBil1** chromophore undergoes intersystem crossing to the triplet manifold. This behavior has been previously observed for conventional tetrapyrrole porphyrinoids.[63] Moreover, this rationale is consistent with the decreased fluorescence quantum yield observed for **Zn**[**DMBil1**] as compared to the free base ligand. Irradiation of CH_3OH solutions of **Cu**[**DMBil1**] led to negligible production of $^1O_2$ ($\Phi_{^1O_2} < 0.2 \times 10^{-2}$) upon irradiation at λ_{irr} = 500 nm, consistent with rapid relaxation of the excited state of this complex via the low-energy copper d−d states.

CONCLUDING REMARKS

Linear tetrapyrrole architectures have interesting redox, spectroscopic, and photophysical properties. To date, however, the pace at which such systems have been prepared and studied has significantly lagged behind that of macrocyclic porphyrinoids. This discrepancy is due in part to the arduous synthesis and inherent instability of a,c-biladienes and other linear tetrapyrroles. Substitution of the 10-position of the general biladiene architecture with germinal dimethyl groups allows for the convenient construction, isolation, and study of a 10,10-dimethylbiladiene platform with pentafluorophenyl substituents at the 5- and 15-*meso* positions (**DMBIl1**). Moreover, the straightforward synthesis and excellent stability of **DMBIL1** lends itself to the study and use of this tetrapyrrole scaffold as a ligand for transition-metal centers such as Zn^{2+} (**Zn**[**DMBil1**]) and Cu^{2+} (**Cu**[**DMBil1**]).

Structural analysis confirms that **DMBil1** binds a single metal center within the tetrapyrrole core. Additionally, **DMBil1** and its Zn^{2+} (**Zn**[**DMBil1**]) and Cu^{2+} (**Cu**[**DMBil1**]) derivatives support multiple redox states. Each of these 10,10-dimethylbiladiene derivatives can be both oxidized and reduced by two electrons as judged by CV. Furthermore, **DMBil1** strongly absorbs light in the visible region, and the **Zn**[**DMBil1**] and **Cu**[**DMBil1**] complexes are able to collect photons at wavelengths approaching 600 nm. The ability of these tetrapyrrole systems to sensitize the formation of $^1O_2$ at wavelengths longer than 500 nm was probed. Both the free base and Zn^{2+} 10,10-dimethylbiladiene architectures show modest efficiencies for $^1O_2$ sensitization, demonstrating that the **DMBil1** framework may be a competent platform for the construction of new PDT agents. With these results in hand, we are now poised to further develop the coordination chemistry of **DMBil1** and to investigate these and related nonmacrocyclic tetrapyrrole species for various applications in the photochemical and catalysis arenas.

ASSOCIATED CONTENT

Supporting Information

Spectroscopic, computational, and crystallographic data. This material is available free of charge via the Internet at http://pubs.acs.org. Crystallographic data are also available from the Cambridge Crystallographic Data Centre (CCDC 996931-996933).

AUTHOR INFORMATION

Corresponding Author

*E-mail: joelr@udel.edu. Tel: 302-831-0716.

Author Contributions

The manuscript was written through contributions of all authors. All authors have given approval to the final version of the manuscript.

Notes

The authors declare no competing financial interest.

ACKNOWLEDGMENTS

J.R. thanks Oak Ridge Associated Universities for a Ralph E. Powe Junior Faculty Enhancement Award. Additional financial support for this work was provided in part by the American Chemical Society Petroleum Research Fund and NSF CAREER Award CHE1352120. Work by D.A.L. and Y.-Z.M. was supported by the U.S. Department of Energy, Office of Science, Basic Energy Sciences, Chemical Sciences, Geosciences, and Biosciences Division. NMR and other data were acquired at UD using instrumentation obtained with assistance from the NSF and NIH (NSF MIR 0421224, NSF CRIF MU CHE0840401 and CHE0541775, NIH P20 RR017716).

REFERENCES

(1) Milgrom, L. R. *The Colours of Life: An Introduction to the Chemistry of Porphyrins and Related Compounds*; Oxford University Press: New York, 1997.

(2) Braslavsky, S. E.; Holzwarth, A. R.; Schaffner, K. Solution Conformations, Photophysics, and Photochemistry of Bile Pigments; Bilirubin and Biliverdin, Dimethyl Esters and Related Linear Tetrapyrroles. *Angew. Chem., Int. Ed.* **1983**, *22*, 656−674.

(3) Gossauer, A.; Engel, J. Linear Polypyrrolic Compounds. In *The Porphyrins*, Part B; Dolphin, D., Ed.; Academic Press: New York, 1978.

(4) *Phytochrome and Photoregulation in Plants*; Furuya, M., Ed.; Academic Press: New York, 1987.

(5) Bonfiglio, J. V.; Bonnett, R.; Buckley, D. G.; Hamzetash, D.; Hursthouse, M. B.; Malik, K. M. A.; et al. Linear Tetrapyrroles As Ligands: Syntheses and X-ray Analyses of Boron and Nickel Complexes of Octaethyl-21H,24H-bilin-1,19-dione. *Tetrahedron* **1983**, *39*, 1865−1874.

(6) Balch, A. L.; Mazzanti, M.; Noll, B. C.; Olmstead, M. M. Geometric and Electronic Structure and Dioxygen Sensitivity of the Copper Complex of Octaethylbilindione, a Biliverdin Analog. *J. Am. Chem. Soc.* **1993**, *115*, 12206−12207.

(7) Koerner, R.; Olmstead, M. M.; Ozarowski, A.; Balch, A. L. A Linear Tetrapyrrole as a Binucleating Ligand with Copper(II). Coordination beyond the Usual $M-N_4$ Bonding. *Inorg. Chem.* **1999**, *38*, 3262−3263.

(8) Koerner, R.; Olmstead, M. M.; Ozarowski, A.; Phillips, S. L.; Van Calcar, P. M.; Winkler, K.; Balch, A. L. Possible Intermediates in Biological Metalloporphyrin Oxidative Degradation. Nickel, Copper, and Cobalt Complexes of Octaethylformybiliverdin and Their Conversion to a Verdoheme. *J. Am. Chem. Soc.* **1998**, *120*, 1274−1284.

(9) Lord, P. A.; Olmstead, M. M.; Balch, A. L. Redox Characteristics of Nickel and Palladium Complexes of the Open-Chain Tetrapyrrole Octaethylbilindione: A Biliverdin Model. *Inorg. Chem.* **2000**, *39*, 1128−1134.

(10) Attar, S.; Balch, A. L.; Van Calcar, P. M.; Winkler, K. Electron Transfer Behavior and Solid State Structures of the Helical Cobalt Complexes of the Open-Chain Tetrapyrrole Ligand, Octaethylbilindione. *J. Am. Chem. Soc.* **1997**, *119*, 3317−3323.

(11) Koerner, R.; Olmstead, M. M.; Van Calcar, P. M.; Winkler, K.; Balch, A. L. Carbon Monoxide Production during the Oxygenation of Cobalt Complexes of Linear Tetrapyrroles. Formation and Characterization of Co^{II}(tetraethylpropentdyopent anion)$_2$. *Inorg. Chem.* **1998**, *37*, 982−988.

(12) Lord, P. A.; Noll, B. C.; Olmstead, M. M.; Balch, A. L. A Remarkable Skeletal Rearrangement of a Coordinated Tetrapyrrole: Chemical Consequences of Palladium π-Coordination to a Bilindione. *J. Am. Chem. Soc.* **2001**, *123*, 10554−10559.

(13) Antina, E. V.; Gusev, G. B.; Rumyantsev, E. V.; Dudina, N. A. Thermal Properties of Ligands, Salts and Metal Complexes of Linear Oligopyrroles. *Russ. J. Gen. Chem.* **2009**, *79*, 1900−1909.

(14) Pandey, R. K.; Zhou, H.; Gerzevske, K.; Smith, K. M. Stepwise Synthesis of 1,19-Dibromo-a,c-biladienes and Their Conversion into Biliverdins, Corroles and Azaporphyrins. *Chem. Commun.* **1992**, 183−185.
(15) Singh, J. P.; Xie, L. Y.; Dolphin, D. An Improved Synthesis of Monoazaporphyrins. *Tetrahedron Lett.* **1995**, *36*, 1567−1570.
(16) Neya, S.; Sato, T.; Hoshino, T. A Concise Synthesis of Monoazaporphyrin from 1,19-Dideoxybiladiene-ac. *Tetrahedron Lett.* **2008**, *49*, 1613−1615.
(17) Paolesse, R.; Froiio, A.; Nardis, S.; Mastroianni, M.; Russo, M.; Nurco, D. J.; Smith, K. M. Novel Aspects of the Chemistry of 1,19-Diunsubstituted a,c-Biladienes. *J. Porphyrins Phthalocyanines* **2003**, *07*, 585−592.
(18) Van Norman, J. D. Electroanalytical and Spectral Study of Bilirubin in Dimethyl Formamide. *Anal. Chem.* **1973**, *45*, 173−175.
(19) Dolphin, D.; Johnson, A. W.; Leng, J.; van den Broek, P. The Base-Catalysed Cyclisations of 1,19-Dideoxybiladienes-ac. *J. Chem. Soc. C* **1966**, 880−884.
(20) Genokhova, N. S.; Melent'eva, T. A.; Berezovskii, V. M. Synthesis of Corroles and Octadehydrocorrins. *Russ. Chem. Rev.* **1980**, *49*, 1056−1067.
(21) Dolphin, D.; Harris, R. L. N.; Huppatz, J. L.; Johnson, A. W.; Kay, I. T.; Leng, J. The Synthesis of 5,5-bi-(Dipyrromethenyls) and Related Compounds. *J. Chem. Soc. C* **1966**, 98−106.
(22) Pistner, A. J.; Yap, G. P. A.; Rosenthal, J. A Tetrapyrrole Macrocycle Displaying a Multielectron Redox Chemistry and Tunable Absorbance Profile. *J. Phys. Chem. C* **2012**, *116*, 16918−16924.
(23) O'Brien, A. Y.; McGann, J. P.; Geier, G. R., III. Dipyrromethane + Dipyrromethanedicarbinol Routes to an Electron Deficient meso-Substituted Phlorin with Enhanced Stability. *J. Org. Chem.* **2007**, *72*, 4084−4092.
(24) Pistner, A. J.; Lutterman, D. A.; Ghidiu, M. J.; Ma, Y.-Z.; Rosenthal, J. Synthesis, Electrochemistry, and Photophysics of a Family of Phlorin Macrocycles That Display Cooperative Fluoride Binding. *J. Am. Chem. Soc.* **2013**, *135*, 6601−6607.
(25) Pistner, A. J.; Lutterman, D. A.; Ghidiu, M. J.; Walker, E.; Yap, G. P. A.; Rosenthal, J. Factors Controlling the Spectroscopic Properties and Supramolecular Chemistry of an Electron Deficient 5,5-Dimethylphlorin Architecture. *J. Phys. Chem. C* **2014**, *118*, 14124−14132.
(26) Harmjanz, M.; Gill, H. S.; Scott, M. J. Porphodimethene−Porphyrin Interconversion: A Tetrapyrrolic Redox-Switchable Macrocycle. *J. Am. Chem. Soc.* **2000**, *122*, 10476−10477.
(27) Harmjanz, M.; Scott, M. J. Facile Synthesis of Stacked, Heteronuclear Porphyrin Arrays with Varied Architechtures. *Inorg. Chem.* **2000**, *39*, 5428−5429.
(28) Korobkov, I.; Gambarotta, S.; Yap, G. P. A. A Highly Reactive Uranium Complex Supported by the Calix[4]tetrapyrrole Tetraanion Affording Dinitrogen Cleavage, Solvent Deoxygenation, and Polysilanol Depolymerization. *Angew. Chem., Int. Ed.* **2002**, *41*, 3433−3436.
(29) Bachmann, J.; Nocera, D. G. Multielectron Chemistry of Zinc Porphyrinogen: A Ligand-Based Platform for Two-Electron Mixed Valency. *J. Am. Chem. Soc.* **2004**, *126*, 2829−2837.
(30) Pangborn, A. B.; Giardello, M. A.; Grubbs, R. H.; Rosen, R. K.; Timmers, F. J. Safe and Convenient Procedure for Solvent Purification. *Organometallics* **1996**, *15*, 1518−1520.
(31) Gottlieb, H. E.; Kotlyar, V.; Nudelman, A. NMR Chemical Shifts of Common Laboratory Solvents as Trace Impurities. *J. Org. Chem.* **1997**, *62*, 7512−7515.
(32) Brouwer, A. M. Standards for Photoluminescence Quantum Yield Measurements in Solution. *Pure Appl. Chem.* **2011**, *83*, 2213−2228.
(33) Calvert, J. M.; Caspar, J. V.; Binstead, R. A.; Westmoreland, T. D.; Meyer, T. J. Metallopolymer Photochemistry. Photophysical, Photochemical and Photoelectrochemical Properties of $(bpy)_2Ru^{II}$ Sites Bound to Poly(4-vinylpyridine). *J. Am. Chem. Soc.* **1982**, *104*, 6620−6627.
(34) Teesdale, J. J.; Pistner, A. J.; Yap, G. P. A.; Ma, Y.-Z.; Lutterman, D. A.; Rosenthal, J. Reduction of CO_2 Using a Rhenium Bipyridine Complex Containing Ancillary BODIPY Moieties. *Catal. Today* **2014**, *225*, 149−157.
(35) Liu, Y.; Hammitt, R.; Lutterman, D. A.; Joyce, L. E.; Thummel, R. P.; Turro, C. Ru(II) Complexes of New Tridentate Ligands: Unexpected High Yield of Sensitized $^1O_2$. *Inorg. Chem.* **2009**, *48*, 375−385.
(36) Noviandri, I.; Brown, K. N.; Fleming, D. S.; Gulyas, P. T.; Lay, P. A.; Masters, A. F.; Philips, L. The Decamethylferrocenium/Decamethylferrocene Redox Couple: A Superior Redox Standard to the Ferrocenium/Ferrocene Redox Couple for Studying Solvent Effects on the Thermodynamics of Electron Transfer. *J. Phys. Chem. B* **1999**, *103*, 6713−6722.
(37) Sheldrick, G. M. A Short History of SHELX. *Acta Crystallogr.* **2008**, *A64*, 112−122.
(38) Spek, A. L. Single-Crystal Structure Validation with the Program PLATON. *J. Appl. Crystallogr.* **2003**, *36*, 7−13.
(39) Frisch, M. J.; Trucks, G. W.; Schlegel, H. B.; Scuseria, G. E.; Robb, M. A.; Cheeseman, J. R.; Scalmani, G.; Barone, V.; Mennucci, B.; Petersson, G. A.; et al. *Gaussian 09*, revision A.1; Gaussian, Inc.: Wallingford, CT, 2009.
(40) Becke, A. D. Density-Functional Thermochemistry. III. The Role of Exact Exchange. *J. Chem. Phys.* **1993**, *98*, 5648−5652.
(41) Becke, A. D. Density-Functional Exchange-Energy Approximation with Correct Asymptotic Behavior. *Phys. Rev. A* **1988**, *38*, 3098−3100.
(42) Lee, C.; Yang, W.; Parr, R. G. Development of the Colle−Salvetti Correlation-Energy Formula into a Functional of the Electron Density. *Phys. Rev. B* **1988**, *37*, 785−789.
(43) Hay, P. J.; Wadt, W. R. Ab Initio Effective Core Potentials for Molecular Calculations. Potentials for Main Group Elements Na to Bi. *J. Chem. Phys.* **1985**, *82*, 284−298.
(44) Marenich, A. V.; Cramer, C. J.; Truhlar, D. G. Universal Solvation Model Based on Solute Electron Density and on a Continuum Model of the Solvent Defined by the Bulk Dielectric Constant and Atomic Surface Tensions. *J. Phys. Chem. B* **2009**, *113*, 6378−6396.
(45) Licoccia, S. L.; Di Vona, M. L.; Paolesse, R. Acid-Catalyzed Cyclization of 1,19-Unsubstituted a,c-Bilidienes. *J. Org. Chem.* **1998**, *63*, 3190−3195.
(46) Struckmeier, G.; Thewalt, U.; Fuhrhop, J. H. Structures of Zinc Octaethyl Formylbiliverdinate Hydrate and Its Dehydrated Bis-Helical Dimer. *J. Am. Chem. Soc.* **1976**, *98*, 278−279.
(47) Sheldrick, W. S.; Engel, J. Zinc Complex of 1,2,3,7,8,12,13,17,18,19-Decamethylbiladiene-a,c. *Acta Crystallogr., Sect. B* **1981**, *37*, 250−252.
(48) Whitten, D. Photochemistry of Porphyrins and Their Metal Complexes in Solution and Organized Media. *Rev. Chem. Intermed.* **1978**, *2*, 107−138.
(49) Bonnett, R. Photosensitizers of the Porphyrin and Phthalocyanine Series for Photodynamic Therapy. *Chem. Soc. Rev.* **1995**, *24*, 19−33.
(50) O'Connor, A. E.; Gallagher, W. M.; Byrne, A. T. Porphyrin and Nonporphyrin Photosensitizers in Oncology: Preclinical and Clinical Advances in Photodynamic Therapy. *Photochem. Photobiol.* **2009**, *85*, 1053−1074.
(51) Nyman, E. S.; Hynninen, P. H. Research Advances in the Use of Tetrapyrrolic Photosensitizers for Photodynamic Therapy. *J. Photochem. Photobiol., B* **2004**, *73*, 1−28.
(52) Pandey, R. K.; Smith, K. M.; Dougherty, T. J. Porphyrin Dimers as Photosensitizers in Photodynamic Therapy. *J. Med. Chem.* **1990**, *33*, 2032−2038.
(53) Ethirajan, M.; Chen, Y.; Joshi, P.; Pandey, R. K. The Role of Porphyrin Chemistry in Tumor Imaging and Photodynamic Therapy. *Chem. Soc. Rev.* **2011**, *40*, 340−362.
(54) Detty, M. R.; Gibson, S. L.; Wagner, S. J. Current Clinical and Preclinical Photosensitizers for Use in Photodynamic Therapy. *J. Med. Chem.* **2004**, *47*, 3897−3915.
(55) Brandis, A.; Mazor, O.; Neumark, E.; Rosenbach-Belkin, V.; Salomon, Y.; Scherz, A. Novel Water-Soluble Bacteriochlorophyll

Derivatives for Vascular-Targeted Photodynamic Therapy: Synthesis, Solubility, Phototoxicity and the Effect of Serum Proteins. *Photochem. Photobiol.* **2005**, *81*, 983−992.
(56) Senge, M. O.; Brandt, J. C. Temoporfin (Foscan®, 5,10,15,20-Tetra(m-hydroxyphenyl)chlorin)—A Second-Generation Photosensitizer. *Photochem. Photobiol.* **2011**, *87*, 1240−1296.
(57) Kessel, D.; Woodburn, K.; Gomer, C. J.; Jagerovic, N.; Smith, K. M. Photosensitization with Derivatives of Chlorin p6. *J. Photochem. Photobiol., B* **1995**, *28*, 13−18.
(58) Zenkevich, E.; Sagun, E.; Knyukshto, V.; Shulga, A.; Mironov, A.; Efremova, O.; Bonnett, R.; Songca, S. P.; Kassem, M. Photophysical and Photochemical Properties of Potential Porphyrin and Chlorin Photosensitizers for PDT. *J. Photochem. Photobiol., B* **1996**, *33*, 171−180.
(59) Sternberg, E. D.; Dolphin, D.; Brückner, C. Porphyrin-Based Photosensitizers for use in Photodynamic Therapy. *Tetrahedron* **1998**, *54*, 4151−4202.
(60) Bhattacharyya, K.; Das, P. K. Qualitative Aspects of All-trans-Retinol Singlet and Triplet Quenching by Oxygen. *Chem. Phys. Lett.* **1985**, *116*, 326−332.
(61) Young, R. H.; Wehrly, K.; Martin, R. L. Solvent Effects in Dye-Sensitized Photooxidation Reactions. *J. Am. Chem. Soc.* **1971**, *93*, 5774−5779.
(62) Kalyanasundaram, K. *Photochemistry of Polypyridine and Porphyrin Complexes*; Academic Press: London, 1992; p 476.
(63) Harriman, A. Luminescence of Porphyrins and Metalloporphyrins. Part 1. — Zinc(II), Nickel(II) and Manganese(II) Porphyrins. *Faraday Trans.* **1980**, *76*, 1978−1985.